A tumor-targeted immune checkpoint blocker

Yuhan Zhang[a,1], Changming Fang[b,1], Rongsheng E. Wang[c], Ying Wang[b], Hui Guo[a], Chao Guo[a,d], Lijun Zhao[e], Shuhong Li[e], Xia Li[d], Peter G. Schultz[b,c,2], Yu J. Cao[e,2], and Feng Wang[a,2]

[a]Key Laboratory of Protein and Peptide Pharmaceuticals, Institute of Biophysics, Chinese Academy of Sciences, 100101 Beijing, China; [b]California Institute for Biomedical Research (Calibr), La Jolla, CA 92037; [c]Department of Chemistry, The Scripps Research Institute, La Jolla, CA 92037; [d]School of Ocean, Shandong University, 264209 Weihai, China; and [e]State Key Laboratory of Chemical Oncogenomics, Key Laboratory of Chemical Genomics, Peking University Shenzhen Graduate School, 518055 Shenzhen, China

Contributed by Peter G. Schultz, June 7, 2019 (sent for review April 3, 2019; reviewed by Peter S. Kim and David A. Spiegel)

To direct checkpoint inhibition to the tumor microenvironment, while avoiding systemic immune activation, we have synthesized a bispecific antibody [norleucine4, D-Phe7]-melanocyte stimulating hormone (NDP-MSH)-antiprogrammed cell death-ligand 1 antibody (αPD-L1) by conjugating a melanocyte stimulating hormone (α-MSH) analog to the antiprogrammed cell death-ligand 1 to (αPD-L1) antibody avelumab. This bispecific antibody can bind to both the melanocortin-1 receptor (MC1R) and to PD-L1 expressed on melanoma cells and shows enhanced specific antitumor efficacy in a syngeneic B16-SIY melanoma mouse model compared with the parental antibody at a 5 mg/kg dose. Moreover, the bispecific antibody showed increased infiltrated T cells in the tumor microenvironment. These results suggest that a tumor-targeted PD-L1-blocking bispecific antibody could have a therapeutic advantage in vivo, especially when used in combination with other checkpoint inhibitors.

bispecific antibody | immunotherapy | PD-L1 inhibitor | melanoma

A major focus of cancer drug development is the generation of therapeutics that block immune escape by cancer cells. A number of antibodies modulating immune checkpoints have been approved as drugs (1–4). The anticytotoxic T lymphocyte antigen-4 antibody ipilimumab was approved for the treatment of melanoma in 2011 (5), and the antiprogrammed cell death-1 (PD-1) antibodies nivolumab and pembrolizumab were approved for advanced melanoma and nonsmall cell lung cancer (NSCLC) in 2014 (6–9), respectively. The clinical efficacy of these antibodies is impressive—ipilimumab and pembrolizumab have raised the 3-y survival of patients with melanoma to ∼70% and overall survival (>5 y) to ∼30% (10).

However, the success of these therapies is somewhat dampened by the lack of response in many patients. For example, in advanced-stage NSCLC and SCLC, only 15–20% of patients treated with PD-1 or PD-L1 targeted antibodies have effective and durable responses (10, 11). To overcome these drawbacks, several approaches have been pursued including combining 2 different immune checkpoint blocking antibodies to increase response rates, and combining immunotherapy with chemotherapy or radiotherapy to enhance clinical efficacy (1–4, 12, 13). However, current immune checkpoint inhibitors are not tumor specific and induce systemic immune activation in other tissues and organs (14, 15). Combination immunotherapies further amplify these toxicities, e.g., treatment with a combination of ipilimumab and nivolumab increased the occurrence of severe side effects by 2- to 4-fold compared with the monotherapies alone (16).

We hypothesized that targeted immunotherapy, i.e., introduction of a tumor-specific targeting element into immune checkpoint blockers, should decrease damage to normal tissues caused by systemic immune responses, resulting in an improved therapeutic index and facilitating combination checkpoint therapies. In this study, we report the generation and preliminary biological characterization of a melanocortin-1 receptor (MC1R) targeted αPD-L1 antibody. This bispecific antibody binds tumor cells in a dual-targeting manner, directing the antibody to melanoma cells while reversing immune suppression in the tumor environment. Our in vivo results demonstrate the potential utility of bispecific antibodies for the tumor-targeted delivery of immune checkpoint blockers.

Results and Discussion

Construction of NDP-MSH-αPD-L1 Conjugate. As a marker of melanoma risk, MC1R is expressed at high levels in more than 80% of human melanomas (17, 18). Over the years, radiolabeled α-MSH (a natural ligand of MC1R) and its analogs have been used for melanoma imaging and treatment (19–21). Therefore, we initially selected α-MSH as a targeting agent, and conjugated α-MSH analogs to the αPD-L1 monoclonal antibody avelumab (22). To generate a bispecific antibody, a potent analog, [norleucine4, D-Phe7]-melanocyte stimulating hormone (NDP-MSH), with a PEG linker (azido-PEG24-SYS-Nle-EHfRWGKPV-CONH2, Nle = norleucine, and f = D-form Phe) was synthesized (Fig. 1). This biologically stable synthetic MSH analog was approved in Europe in 2015 to prevent UV skin damage in people with erythropoietic protoporphyria and has a higher binding affinity to MC1R than α-MSH (0.67 ± 0.09 vs. 2.58 ± 0.33 nM), which helps overcome in vivo competition by endogenous ligand (17, 20, 23). This peptide showed high shelf stability and good biological stability in vivo (24). A peptide with a similar but nonbinding sequence was also synthesized and used as a control (NR, azido-PEG24-SEGYHKSfRP-Nle-WV-CONH2). The human IgG1 αPD-L1

Significance

Current immune checkpoint inhibitors are not tumor specific and induce systemic immune activation in other tissues and organs. Combination immunotherapies further amplify these toxicities, which limit their clinical application. Here, we describe a strategy to direct checkpoint inhibition to the tumor microenvironment while avoiding systemic immune activation. Specifically, we have synthesized a bispecific antibody by conjugating an MSH analog to the αPD-L1 antibody avelumab. This bispecific antibody binds both MC1R and PD-L1 on cancer cells, shows excellent in vitro activities, and has enhanced efficacy in a syngeneic melanoma mouse model as compared to the parental antibody. This work demonstrates that the incorporation of a targeting element into an immune checkpoint blocking antibody could provide a therapeutic advantage.

Author contributions: Y.Z., C.F., R.E.W., P.G.S., Y.J.C., and F.W. designed research; Y.Z., C.F., R.E.W., Y.W., H.G., C.G., L.Z., S.L., and Y.J.C. performed research; Y.Z., C.F., H.G., X.L., P.G.S., Y.J.C., and F.W. analyzed data; and Y.Z., C.F., P.G.S., and F.W. wrote the paper.

Reviewers: P.S.K., Stanford University and Chan Zuckerberg Biohub; and D.A.S., Yale University.

The authors declare no conflict of interest.

[1]Y.Z. and C.F. contributed equally to this work.

[2]To whom correspondence may be addressed. Email: schultz@scripps.edu, joshuacao@pku.edu.cn, or wangfeng@ibp.ac.cn.

This article contains supporting information online at www.pnas.org/lookup/suppl/doi:10.1073/pnas.1905646116/-/DCSupplemental.

Published online July 22, 2019.

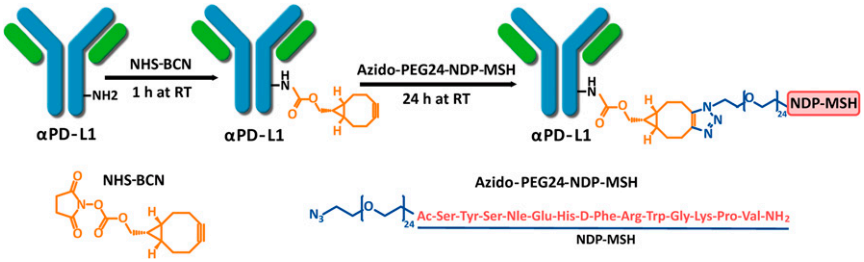

Fig. 1. Synthesis of NDP-MSH-αPD-L1 antibody-peptide conjugate.

antibody avelumab is human and mouse cross reactive (K_d = 0.3 and 1 nM, respectively) (25) and, therefore, was chosen as the antibody backbone. Heavy and light chain genes of avelumab were cloned into the pFuse vector and coexpressed by transient transfection in FreeStyle 293F cells in a yield of 30 mg/L. SDS/PAGE analysis revealed >90% purity (Fig. 2*A*). After reduction by DTT, the light chain migrated at 25 kDa, and the heavy chain migrated at 50 kDa matching the calculated molecular mass of heavy and light chains.

The αPD-L1/NDP-MSH (NDP-MSH-αPD-L1) bispecific antibody was generated by nonspecifically conjugating a NHS ester of NDP-MSH to lysine residues of the αPD-L1 antibody by a 2-step ligation (Fig. 1). Briefly, NHS-bicyclo[6.1.0]non-4-yn-9-ylmethyl (BCN) was conjugated to the primary amine of exposed lysines of αPD-L1 antibody (1 mg/mL) in PBS at pH 8.3 for 1 h at room temperature to form stable amide bonds. After removing unreacted NHS-BCN using a desalting column, the BCN-conjugated αPD-L1 antibody (0.8 mg/mL) was then reacted with azido-PEG24-NDP-MSH (or -NR) by a catalyst-free "click reaction" in a 1:20 molar ratio at pH 7.0 and 37 °C for 24 h. The product was purified by size-exclusion chromatography to remove excess nonconjugated NDP-MSH peptide (*SI Appendix*, Fig. S1). The antibody conjugates were analyzed by SDS/PAGE under reducing and nonreducing conditions. After reduction by DTT, the light chains migrated at 25–35 kDa, and the heavy chains migrated at 50–65 kDa in the form of multiple bands with an ∼3 kDa increment between each band (Fig. 2*A*). The antibody is 90% conjugated with stoichiometries ranging from 1 to 8 MSH-peptide/antibody as determined by mass spectrometry analysis with expected molecular weights. The average MSH LAR is about 3.5 based on mass spectroscopy analysis (Fig. 2 *B* and *C*). The NR-αPD-L1 was generated and analyzed by the same methods. The overall yields for the purified conjugated product range from 30 to 40%, and the conjugate can be concentrated to 12 mg/mL without aggregation.

In Vitro Activities of NDP-MSH-αPD-L1 Conjugate. Next, we characterized the binding of the conjugate to its respective receptors. NDP-MSH-αPD-L1 and NR-αPD-L1 show nearly the same binding affinity (EC_{50} = 0.17 ± 0.02 and 0.18 ± 0.01 nM, respectively) to a human PD-L1 (extracellular domain)-Fc fusion protein by ELISA as that of the αPD-L1 antibody alone (EC_{50} = 0.19 ± 0.01 nM) (Fig. 3*A*). This result indicates that a LAR = 3.5 does not significantly affect binding of the conjugated antibody to PD-L1. The binding of NDP-MSH-αPD-L1 to human MC1R was analyzed by cell surface ELISA with a HEK293 cell line that overexpresses human MC1R (23).

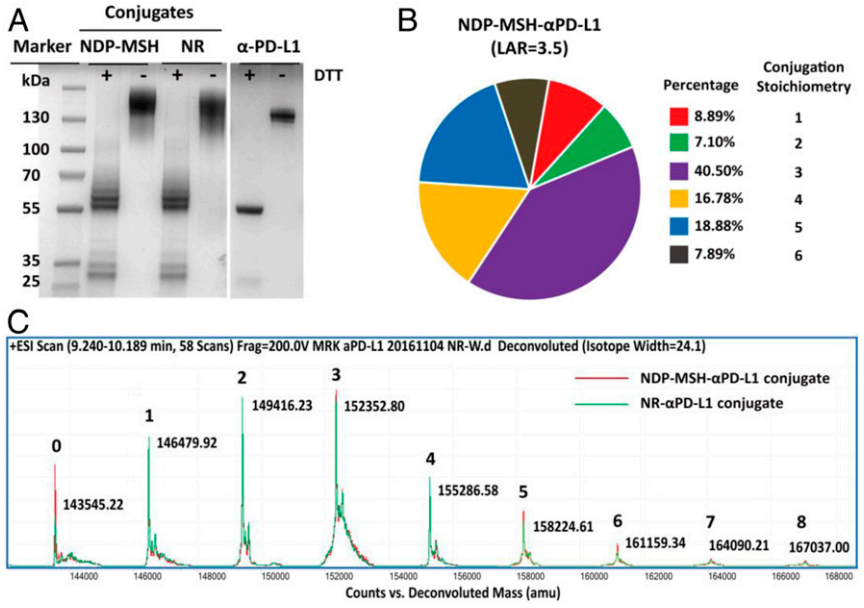

Fig. 2. Characterization of anti-PD-L1 antibody and antibody conjugates. (*A*) Characterization of anti-PD-L1 antibody, NDP-MSH-αPD-L1, and anti-PD-L1/NR (NR-αPD-L1) conjugates with SDS/PAGE. Proteins were loaded with or without 50 μM DTT reduction. (*B*) The overall ligand-antibody ratio (LAR) for the MSH-αPD-L1 conjugate was 3.5. The distribution of the conjugation sites of NDP-MSH-αPD-L1 was determined by mass spectrometry (MS). (*C*) Electrospray ionization–MS (ESI–MS) analysis of the molecular weight distribution of NDP-MSH-αPD-L1 and NR-αPD-L1 conjugates. The *N*-gylcans were removed by incubation with PNGase F (Promega, PBS pH 7.4, 37 °C, and 12 h).

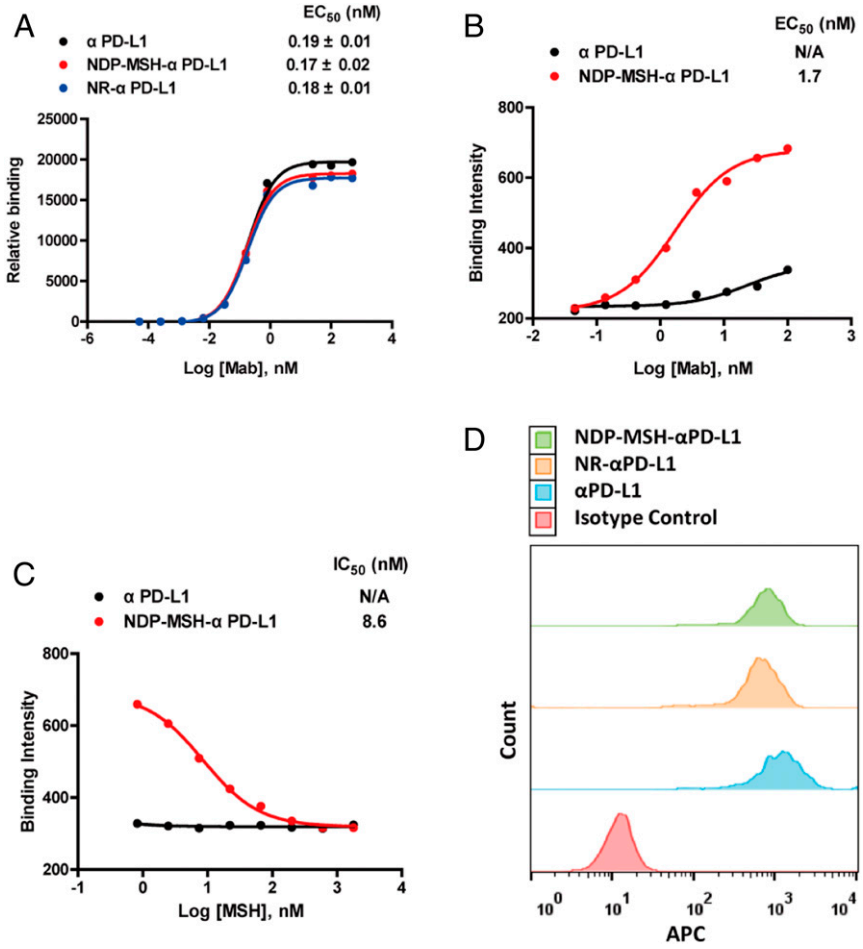

Fig. 3. In vitro activities of NDP-MSH-αPD-L1 conjugates. (*A*) Binding of NDP-MSH-αPD-L1, NR-αPD-L1, and αPD-L1 to Fc-fused human PD-L1 extracellular domain was detected by a HRP-labeled polyclonal antihuman κ light chain antibody using an ELISA. Error bars represent SD of duplicate samples. (*B*) NDP-MSH-αPD-L1 conjugates bound to the cell surface of HEK293-MC1R ($MC1R^+/PD\text{-}L1^-$) cells in a cell surface ELISA in a dose-dependent fashion. (*C*) The binding of NDP-MSH-αPD-L1 (30 nM) to HEK293-MC1R cells was completed by free MSH peptide dose dependently. (*D*) NDP-MSH-αPD-L1 and control antibodies bound to PD-L1 expressing murine melanoma cells B16-SIY ($MC1R^+/PD\text{-}L1^+$). Binding was detected by allophycocyanin labeled antihuman IgG secondary antibody.

NDP-MSH-αPD-L1 bound HEK293-MC1R cells in a dose-dependent manner (EC_{50} = 1.72 ± 0.31 nM) (Fig. 3*B*), and this specific binding was completed by a free MSH peptide (Fig. 3*C*). The activities of the NDP-MSH-αPD-L1 conjugates were also examined using HEK293 cells overexpressing MC1R and carrying a cAMP response element (CRE) luciferase (Luc) reporter. Cell surface MC1Rs were activated by NDP-MSH-αPD-L1 dose dependently, and downstream signal transduction was induced with an EC_{50} = 2.70 ± 1.03 nM (*SI Appendix*, Fig. S2), similar to the value from the cell surface ELISA. This result indicates that NDP-MSH-αPD-L1 can activate MC1R with nanomolar potency, similar to that of azido-PEG24-NDP-MSH (EC_{50} = 0.94 ± 0.11 nM) but less than that of the NDP-MSH peptide (EC_{50} = 0.09 ± 0.02 nM) in this cell-based reporter assay. Given the similar EC_{50}s of azido-PEG24-NDP-MSH and the antibody conjugate, this reduced affinity to MC1R likely results from the linker at the N terminus of NDP-MSH interfering to some degree with the engagement of MC1R.

Avelumab is cross reactive with human and mouse PD-L1 and, therefore, is suitable for both in vivo efficacy studies in syngeneic mouse models and ultimately human clinical studies (26). Likewise, NDP-MSH binds to both human and mouse MC1R (20, 21). We further confirmed binding of the conjugate NDP-MSH-αPD-L1 to mouse B16-SIYRYYGL (SIY) cells (a melanoma cell line derived from B16) that highly express mouse PD-L1 and MC1R. Incubation of 500 nM αPD-L1 with B16-SIY cells resulted in a peak shift in flow cytometry analysis. Similar binding was observed with NDP-MSH-αPD-L1 and NR-αPD-L1 (Fig. 3*D*). These results demonstrate that the bispecific conjugate can bind both MC1R and PD-L1 in vitro with good affinity and suggests that the B16-SIY mouse melanoma model can be used to investigate its efficacy.

Serum Stability and Pharmacokinetic Analysis of NDP-MSH-αPD-L1 Conjugate. The stability of NDP-MSH-αPD-L1 was examined in freshly collected mouse serum. The concentration of the conjugated antibody was determined by ELISA using a PD-L1-(extracellular domain)-Fc fusion antigen. During 72 h of incubation, no significant degradation was observed (*SI Appendix*, Fig. S3), suggesting that peptide conjugation does not reduce the stability of the antibody in mouse serum. In addition, NDP-MSH-αPD-L1 has a melting temperature at 64 °C in a thermal stability assay, similar to that of αPD-L1 (*SI Appendix*, Fig. S4). We next performed a pharmacokinetic (PK) analysis of NDP-MSH-αPD-L1 in mice, analyzing plasma samples using the same ELISA method described above in serum stability assay. NDP-MSH-αPD-L1, NR-αPD-L1, and the αPD-L1 antibody show a

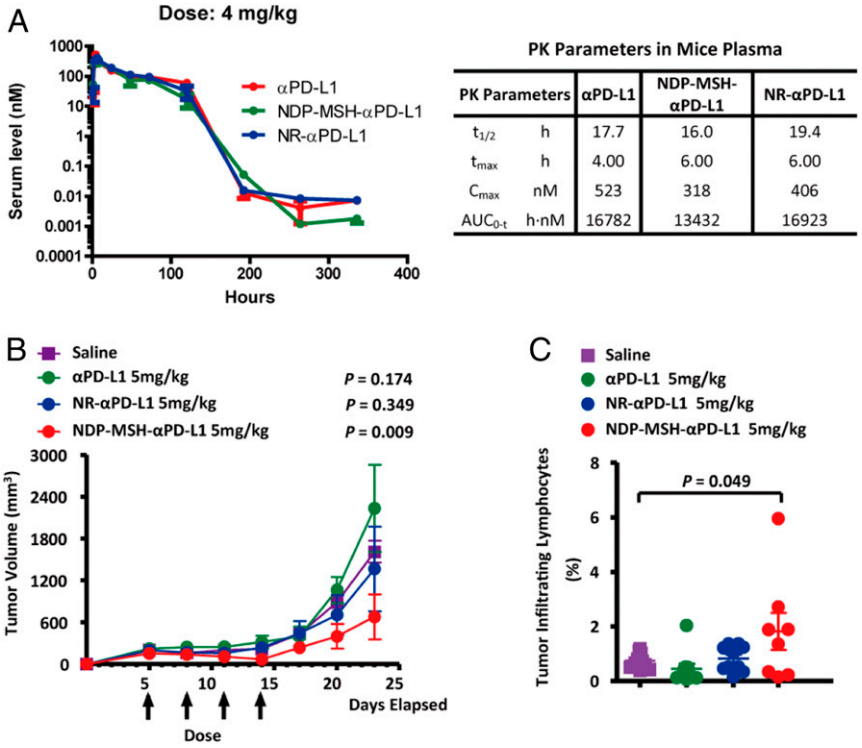

PK Parameters		αPD-L1	NDP-MSH-αPD-L1	NR-αPD-L1
$t_{1/2}$	h	17.7	16.0	19.4
t_{max}	h	4.00	6.00	6.00
C_{max}	nM	523	318	406
AUC_{0-t}	h·nM	16782	13432	16923

Fig. 4. Pharmacokinetics and in vivo efficacy of NDP-MSH-αPD-L1. (*A*) Pharmacokinetics of NDP-MSH-αPD-L1 and controls in the mouse. NDP-MSH-αPD-L1 in PBS or controls was injected intraperitoneally into mice at 4 mg/kg (n = 3/group), and serum was isolated for determination of conjugate concentration. Concentration vs. time curves were evaluated by noncompartmental analysis using WinNonlin. Values shown are averages of 3 mice in the group. $t_{1/2}$, half-life; t_{max}, maximum concentration time; C_{max}, maximum concentration; $AUC_{0\rightarrow inf}$, area under the concentration–time curve extrapolated to infinity. (*B*) In vivo efficacy of NDP-MSH-αPD-L1 in mouse B16-SIY melanoma syngeneic models (n = 10/group). The tumor was measured 3 times a week with calipers, and the tumor volume was calculated. Each data point represents mean tumor volume of 10 mice in each group ± SD. Arrows indicate the time of drug injection. P values < 0.05 compared with the control groups (saline) were considered significant. (*C*) Analysis of tumor infiltrating lymphocytes (TILs). C57BL/6 mice (n = 10/group) were injected with B16-SIY cells and treated with saline or αPD-L1-based drugs on days 5, 8, 11, and 14. On day 14, mouse TILs were harvested and analyzed by flow cytometry with the CD3 cell surface marker. P values < 0.05 compared with the control groups (saline) were considered significant.

similar PK profile after i.p. injection with terminal half-lives ranging from 16 to 19 h (Fig. 4*A*). The PK profile is also similar to the results in previous studies of chimeric αPD-L1 antibodies (27, 28).

In Vivo Efficacy of NDP-MSH-αPD-L1 Conjugate. A B16-F10 murine melanoma-bearing model was utilized for the studies of MC1R-targeted radiotherapies (29–31). B16-SIY cells were derived from B16-F10 expressing an engineered model antigen SIY, which are more immunogenic than B16 cells and responsive to αPD-L1 treatment (32–34). Therefore, we chose B16-SIY cells to develop a mouse $MC1R^+/PD\text{-}L1^+$ melanoma syngeneic model and used it to compare the in vivo efficacy of αPD-L1, NR-αPD-L1, and NDP-MSH-αPD-L1. Specifically, C57BL/6 mice were s.c. inoculated with 1.5×10^6 B16-SIY tumor cells on day 0, and treatment was initiated on day 5 post injection when the tumor volume reached ~100 mm^3. Treatment consisted of 4 i.p. injections every 2 d. Groups of mice were treated at doses of 1 and 5 mg/kg for each construct (n = 10/group). The control group was treated with saline only. As shown in Fig. 4*B*, treatment with NDP-MSH-αPD-L1 exhibited a significant antitumor effect. Mice treated with the 5 mg/kg dose of NDP-MSH-αPD-L1 exhibited a strong tumor growth inhibition (P < 0.05 on days 23). In the 5 mg/kg NDP-MSH-αPD-L1 treatment group, tumor sizes in 80% of mice were under 500 mm^3, and 20% of mice showed tumor regression during the treatment time. In mice treated with 1 mg/kg, tumor growth was slowed for the duration of the treatment (*SI Appendix*, Fig. S5). In contrast, treatment of mice with 5 mg/kg αPD-L1 antibody or NR-αPD-L1 showed no significant antitumor effect beyond that observed with saline only (P = 0.174 and 0.345, respectively, on day 23).

NDP-MSH itself is a potent MC1R agonist, which is known to have proliferative effects on melanocytes and is, therefore, not expected to have an antitumor effect itself (35). Consistent with this notion, we showed that NDP-MSH-αPD-L1 did not exhibit any significant growth inhibition or cytotoxicity effects on B16-SIY cells in cultures where no immune cells were involved (*SI Appendix*, Fig. S6). Even at 700 nM concentration, which is the theoretical C_{max} of a 4 mg/kg dose in mice, NDP-MSH-αPD-L1 did not exhibit any significant effects. Similar results were observed for αPD-L1 and NR-αPD-L1. Puromycin was used as the positive control in the experiments.

To gain a better understanding of how this bispecific antibody reduced tumor load, we examined whether the number of mouse T cells in the tumor environment correlated with tumor growth inhibition by NDP-MSH-αPD-L1. Tumors were harvested on day 23, and cells were isolated from solid tumors by enzymatic digestion. The T cell population within the tumor was analyzed by flow cytometry. After staining with a mouse CD3 surface marker, the results confirmed that a significantly higher percentage of $CD3^+$ T cells accumulated in tumor tissue after 5 mg/kg NDP-MSH-αPD-L1 treatment (1.8 ± 1.9%) compared with groups treated with αPD-L1 (0.45 ± 0.6%) antibody or NR-αPD-L1 (0.8 ± 0.46%) (Fig. 4*C*).

Conclusion

To summarize, we have synthesized a bispecific antibody NDP-MSH-αPD-L1 by peptide-antibody conjugation to demonstrate

the potential utility of tumor-targeted delivery of immune checkpoint blockers. This bispecific antibody retains binding affinity to both MC1R and PD-L1 and displayed similar thermal stability, serum stability, and PK properties to its parental αPD-L1 antibody. We then examined its efficacy in an established B16-SIY melanoma syngeneic mouse model where NDP-MSH-αPD-L1 was shown to be more efficacious than either the αPD-L1 antibody or the NR-αPD-L1. TILs analysis also revealed an increase in the number of infiltrated T cells. Together, this paper demonstrates that the incorporation of a targeting element into an immune checkpoint blocking antibody can enhance antitumor activity relative to antiimmune checkpoint therapy alone. Future studies will focus on combining this bispecific antibody with other checkpoint blockades, comparing the activity of these conjugates with site-specific antibody conjugates, and assesing the effects of the relative affinities of the αPD-L1 and MSH components on efficacy.

Materials and Methods

Chemicals and Peptides. NDP-MSH-αPD-L1 with PEG linker (azido-PEG24-SYS-Nle-EHfRWGKPV-CONH2) and NR-MSH with peptide PEG linker (NR, azido-PEG24-SEGYHKSfRP-Nle-WV-CONH2) was synthetized by Innopep Inc. (1R,8S,9s)-BCN-NHS was purchased from Sigma-Aldrich (Cat# 744867).

Cloning of Antibody Expression Vector. The genes encoding the αPD-L1 antibody heavy chain and light chain variable regions were synthesized by IDT (Coralville, IA) and amplified by PCR using PfuUltra II DNA polymerase (Agilent Technologies, CA). The amplified PCR products were cloned to a pFuse-hIgG1-Fc backbone vector (InvivoGen, CA) using a Gibson assembly kit (NEB, MA). The sequences of the resulting mammalian expression vectors were confirmed by DNA sequencing.

Antibody Expression and Purification. The expression vector containing the heavy and light chains of the antibody were coexpressed by transient transfection in FreeStyle 293-F cells (Thermo Fisher Scientific, IL), according to the manufacturer's protocol. After adding plasmid-293fectin mixture, cells in flasks were shaken at 125 rpm in a 5% CO_2 environment at 37 °C. Culture medium containing secreted proteins was harvested and sterile filtered after 96 h. Antibodies were purified by Protein A chromatography (Thermo Fisher Scientific, IL) and analyzed by SDS/PAGE gel and ESI-Q-TOF protein MS in the presence and absence of DTT.

Generation of Antibody-Peptide Conjugates. NHS-BCN was reacted with primary amine of exposed lysines on the surface of the αPD-L1 antibody (1 mg/mL) in slightly alkaline PBS conditions (pH 8.3) for 1 h at room temperature to yield stable amide bonds. The NHS-BCN to αPD-L1 antibody molar ratio was optimized at 40 to achieve the best conjugation yield. The reaction mix was loaded onto a 40 K MWCO Spin Desalting Column (Thermofisher, Cat# 87766) to separate the BCN-conjugated αPD-L1 antibody from free NHS-BCN. The BCN-conjugated αPD-L1 antibody (0.8 mg/mL) was then mixed with azido-PEG24-NDP-MSH (or -NR) in a 1:20 molar ratio. This reaction was carried on in PBS (pH 7.0) and 37 °C for 24 h during which the BCN moiety was covalently ligated with the azido group on the peptide by copper-free click chemistry with a conjugation efficiency >90% based on MS analysis.

Purification and Characterization of Antibody-Peptide Conjugates. NDP-MSH-αPD-L1 (or NR-) conjugates were purified by FPLC in PBS (pH 7.4) at a 0.4 mL/min flow rate with a size-exclusion column (Superdex 200 10/300 GL, GE Healthcare). UV absorbance at 280 nm was plotted vs. the elution time or elution volume. The LAR was determined by ESI-Q-TOF protein MS.

Measurement of PD-L1 Binding Affinity of NDP-MSH-αPD-L1. A 100 ng/well human PD-L1-Fc fusion (Sino Biological, China) was coated on 96-well ELISA plates in PBS (pH 7.4) overnight at 4 °C, followed by blocking with 2% skim milk in PBS (pH 7.4) for 1 h at 37 °C. After washing with 0.05% Tween-20 in PBS, varied concentrations of NDP-MSH-αPD-L1/NR-αPD-L1/αPD-L1 were added and incubated for 2 h at room temperature. A 1:2,000 diluted HRP-labeled polyclonal antihuman κ light chain antibody (Thermo Fisher Scientific, IL) was then added and incubated for 2 h at room temperature. After washing, fluorescence was developed with a QuantaBlu fluorogenic peroxidase substrate (Thermo Fisher Scientific, IL) and quantified using a Spectramax fluorescence plate reader with excitation at 325 nm and emission at 420 nm. Data were plotted and analyzed in Graphpad Prizm by nonlinear regression in the model of logarithm (agonist) vs. response.

Measurement of MC1R Binding Affinity of NDP-MSH-αPD-L1. HEK293 cells were grown in DMEM with 10% FBS, 1% penicillin, and streptomycin. Cells were transfected with plasmid containing the human MC1R gene using lipofectamine (Life Technologies, MD). The permanently transfected clonal cell line was selected by resistance to G418. MC1R overexpressed cells were cultured on a flat-bottom 96-well plate (black) overnight to allow for attachment (2×10^4/well). After washing with PBS buffer, cells were fixed onto the bottom of wells by spinning down and incubating in 8% paraformaldehyde for 15 min. Varied concentrations of NDP-MSH-αPD-L1 or αPD-L1 were added for binding assays. For competition assays, 30 nM of NDP-MSH-αPD-L1 or αPD-L1 in the presence of various concentrations of MSH was incubated with HEK293 MC1R cells. The other ELISA procedures were the same as those published by Abcam (ICE, ab111542). For the final steps, HRP-labeled antihuman IgG (Fc) antibody (ELITechGroup, Netherlands) was diluted 1:1,000 in blocking buffer (PBS/5%BSA/0.1% Tween-20), and applied for 1 h followed by extensive washing. QuantaBlu fluorogenic peroxidase substrate was then added, and fluorescence signals were obtained as mentioned above.

In Vitro MC1R Activation Assay. HEK293 cells overexpressing a MC1R receptor and a CRE-Luc reporter were grown in DMEM with 10% FBS at 37 °C with 5% CO_2. Cells were seeded in 384-well plates at a density of 5,000 cells per well and treated with various concentrations of conjugates or controls for 24 h at 37 °C with 5% CO_2. Luminescence intensities were then measured using One-Glo (Promega, WI) following the manufacturer's instruction. Data were plotted and analyzed in Graphpad Prizm by nonlinear regression in the model of logarithm (agonist) vs. response.

Flow Cytometry Analysis of Binding to B16-SIY Cell Line. B16-SIY cells were grown in DMEM with 10% FBS, 1% penicillin, and streptomycin. Before analysis, cells were washed with cold PBS (pH7.4) 3 times, blocked with 2% BSA in PBS, and incubated with 500 nM antibody for 1 h at 4 °C. After removing the unbound antibody by washing with 2% BSA in PBS, cells were resuspended with FITC antihuman IgG Fc (KPL, MD) for 1 h at 4 °C with gentle mixing, followed by washing with 2% FBS in PBS and analyzed by a LSR II flow cytometer equipped (Becton Dickinson, NJ). All results were processed with FlowJo software (TreeStar, OR).

In Vivo Efficacy Study of NDP-MSH-αPD-L1 Conjugates. The efficacy study was conducted with 6-wk-old female C57BL/6 mice (Jackson Laboratory, $n = 10$). B16-SIY cells were engineered from melanoma cell line B16F10, a model antigen SIY, which can be recognized by $CD8^+$ T cells. A total of 1.5×10^6 B16-SIY melanoma cells were injected s.c. in the flank of each C57BL/6 mouse on day 0. On day 5 post tumor inoculation, animals were sorted based on tumor volume, and each mouse was dosed i.p. with antibodies or saline for 4 doses, spaced 3 d apart (day 5, day 8, day 11, and day 14) at 1 or 5 mg/kg. Tumors were measured and recorded 3 times a week with calipers. Tumor volume was calculated based on length × 1/2 $(\text{width})^2$. Mice were killed at day 23 after tumor injection. Tumors were harvested for further analysis. All procedures were reviewed and approved by the Laboratory Animal Center of Peking University Shenzhen Graduate School, and were performed using protocols in accordance with the relevant guidelines and regulations.

Analysis of Tumor Infiltrated T Lymphocytes. Tumor cell suspensions were prepared from solid tumors by enzymatic digestion in HBSS (Thermo Fisher Scientific, IL) containing 1 mg/mL collagenase, 0.1 mg/mL DNase I, and 2.5 U/mL of hyaluronidase with constant stirring for 2 h at room temperature. The resulting suspension was passed through a 70 um cell strainer, washed once with HBSS, and resuspended in PBS with 3% BSA to a concentration of 1×10^6 cells/mL for flow cytometric analysis. The frequency of $CD3^+$ T cells was determined by staining FITC-labeled antimouse CD3 antibody (eBioscience, San Diego, CA). Cells were acquired using a LSR II flow cytometer (Becton Dickinson, NJ) and analyzed with FlowJo software (TreeStar, OR). An unpaired *t* test (2-tailed) was used to compare between 2 treatment groups. All statistical evaluations of data were performed using Graph Pad Prism software. Statistical significance was achieved at P values < 0.05.

ACKNOWLEDGMENTS. We thank Jingxin Wang for helpful discussions. The work was supported by funding from Strategic Priority Research Program of the Chinese Academy of Sciences (Grant XDB29040202), Chinese Academy of Sciences Pioneer Hundred Talents Program (A), National Key R&D Program of China (Grant 2017YFA0505400), National Natural Science

Foundation of China (Grants 31741042 and 81872783), Guangdong Natural Science Foundation (Grant 2018A030313916), Shenzhen Science and Technology Innovation Program (Grants JCYJ20170818090043031 and JCYJ20180504165501371), and by Calibr.

1. P. Sharma, J. P. Allison, The future of immune checkpoint therapy. *Science* **348**, 56–61 (2015).
2. D. M. Pardoll, The blockade of immune checkpoints in cancer immunotherapy. *Nat. Rev. Cancer* **12**, 252–264 (2012).
3. R. J. Torphy, R. D. Schulick, Y. Zhu, Newly emerging immune checkpoints: Promises for future cancer therapy. *Int. J. Mol. Sci.* **18**, E2642 (2017).
4. H. Kaplon, J. M. Reichert, Antibodies to watch in 2018. *MAbs* **10**, 183–203 (2018).
5. F. S. Hodi *et al*., Improved survival with ipilimumab in patients with metastatic melanoma. *N. Engl. J. Med.* **363**, 711–723 (2010).
6. S. L. Topalian *et al*., Safety, activity, and immune correlates of anti-PD-1 antibody in cancer. *N. Engl. J. Med.* **366**, 2443–2454 (2012).
7. C. Robert *et al*., Nivolumab in previously untreated melanoma without BRAF mutation. *N. Engl. J. Med.* **372**, 320–330 (2015).
8. E. B. Garon *et al*.; KEYNOTE-001 Investigators, Pembrolizumab for the treatment of non-small-cell lung cancer. *N. Engl. J. Med.* **372**, 2018–2028 (2015).
9. A. Ribas *et al*., P0116 Updated clinical efficacy of the anti-PD-1 monoclonal antibody pembrolizumab (MK-3475) in 411 patients with melanoma. *Eur. J. Cancer* **51**, e24 (2015).
10. J. S. O'Donnell, G. V. Long, R. A. Scolyer, M. W. L. Teng, M. J. Smyth, Resistance to PD1/PDL1 checkpoint inhibition. *Cancer Treat Rev.* **52**, 71–81 (2017).
11. C. M. Balch *et al*., Final version of 2009 AJCC melanoma staging and classification. *J. Clin. Oncol.* **27**, 6199–6206 (2009).
12. H. Kaplon, J. M. Reichert, Antibodies to watch in 2019. *MAbs* **11**, 219–238 **(**2019).
13. K. Adachi, K. Tamada, Immune checkpoint blockade opens an avenue of cancer immunotherapy with a potent clinical efficacy. *Cancer Sci.* **106**, 945–950 (2015).
14. J. R. Nedrow *et al*., Imaging of programmed cell death ligand 1: Impact of protein concentration on distribution of Anti-PD-L1 SPECT agents in an immunocompetent murine model of melanoma. *J. Nucl. Med.* **58**, 1560–1566 (2017).
15. A. Josefsson *et al*., Imaging, biodistribution, and dosimetry of radionuclide-labeled PD-L1 antibody in an immunocompetent mouse model of breast cancer. *Cancer Res.* **76**, 472–479 (2016).
16. N. Abdel-Wahab, M. Shah, M. A. Lopez-Olivo, M. E. Suarez-Almazor, Use of immune checkpoint inhibitors in the treatment of patients with cancer and preexisting autoimmune disease: A systematic review. *Ann. Intern. Med.* **168**, 121–130 (2018).
17. A. A. Rosenkranz, T. A. Slastnikova, M. O. Durymanov, A. S. Sobolev, Malignant melanoma and melanocortin 1 receptor. *Biochemistry (Mosc.)* **78**, 1228–1237 (2013).
18. B. Lee, N. Mukhi, D. Liu, Current management and novel agents for malignant melanoma. *J. Hematol. Oncol.* **5**, 3 (2012).
19. A. N. Eberle, Studies on melanotropin (MSH) receptors of melanophores and melanoma cells. *Biochem. Soc. Trans.* **9**, 37–39 (1981).
20. J. Chen *et al*., Evaluation of an (111)In-DOTA-rhenium cyclized α-MSH analog: A novel cyclic-peptide analog with improved tumor-targeting properties. *J. Nucl. Med.* **42**, 1847–1855 (2001).
21. J. Yang *et al*., ^{68}Ga-DOTA-GGNle-CycMSH$_{hex}$ targets the melanocortin-1 receptor for melanoma imaging. *Sci. Transl. Med.* **10**, eaau4445 (2018).
22. H. L. Kaufman *et al*., Avelumab in patients with chemotherapy-refractory metastatic Merkel cell carcinoma: A multicentre, single-group, open-label, phase 2 trial. *Lancet Oncol.* **17**, 1374–1385 (2016).
23. Y. Yang, M. Chen, G. Ventro, C. M. Harmon, Key amino acid residue in Melanocortin-1 receptor (melanocyte α-MSH receptor) for ligand selectivity. *Mol. Cell. Endocrinol.* **454**, 69–76 (2017).
24. M. E. Hadley *et al*., "Discovery and development of novel melanogenic drugs" in *Integration of Pharmaceutical Discovery and Development: Case Histories*, R. T. Borchardt, R. M. Freidinger, T. K. Sawyer, P. L. Smith, Eds. (Springer US, Boston, MA, 1998), pp. 575–595.
25. J. K. Fallon, A. J. Vandeveer, J. Schlom, J. W. Greiner, Enhanced antitumor effects by combining an IL-12/anti-DNA fusion protein with avelumab, an anti-PD-L1 antibody. *Oncotarget* **8**, 20558–20571 (2017).
26. A. J. Vandeveer *et al*., Systemic immunotherapy of non-muscle invasive mouse bladder cancer with avelumab, an Anti-PD-L1 immune checkpoint inhibitor. *Cancer Immunol. Res.* **4**, 452–462 (2016).
27. R. Deng *et al*., Preclinical pharmacokinetics, pharmacodynamics, tissue distribution, and tumor penetration of anti-PD-L1 monoclonal antibody, an immune checkpoint inhibitor. *MAbs* **8**, 593–603 (2016).
28. B. A. Inman, T. A. Longo, S. Ramalingam, M. R. Harrison, Atezolizumab: A PD-L1-blocking antibody for bladder cancer. *Clin. Cancer Res.* **23**, 1886–1890 (2017).
29. Miao Y *et al*., Melanoma therapy via peptide-targeted {alpha}-radiation. *Clin Cancer Res.* **11**, 5616–5621 (2005).
30. Y. Miao, N. K. Owen, D. R. Fisher, T. J. Hoffman, T. P. Quinn, Therapeutic efficacy of a 188Re-labeled alpha-melanocyte-stimulating hormone peptide analog in murine and human melanoma-bearing mouse models. *J Nucl. Med.* **46**, 121–129 (2005).
31. K. R. Gehlsen, M. J. C. Hendrix, In vitro assay demonstrates similar invasion profiles for B16F1 and B16F10 murine melanoma cells. *Cancer Lett.* **30**, 207–212 (1986).
32. S. Spranger *et al*., Mechanism of tumor rejection with doublets of CTLA-4, PD-1/PD-L1, or IDO blockade involves restored IL-2 production and proliferation of CD8(+) T cells directly within the tumor microenvironment. *J. Immunother. Cancer* **2**, 3 (2014).
33. A. Sivan *et al*., Commensal Bifidobacterium promotes antitumor immunity and facilitates anti-PD-L1 efficacy. *Science* **350**, 1084–1089 (2015).
34. J. Kline, L. Zhang, L. Battaglia, K. S. Cohen, T. F. Gajewski, Cellular and molecular requirements for rejection of B16 melanoma in the setting of regulatory T cell depletion and homeostatic proliferation. *J. Immunol.* **188**, 2630–2642 (2012).
35. Z. Abdel-Malek *et al*., Mitogenic and melanogenic stimulation of normal human melanocytes by melanotropic peptides. *Proc. Natl. Acad. Sci. U.S.A.* **92**, 1789–1793 (1995).